Eur. Phys. J. C (2026) 86:158
https://doi.org/10.1140/epjc/s10052-026-15376-x

THE EUROPEAN PHYSICAL JOURNAL C

Regular Article - Theoretical Physics

Decoupling of solitonic quantum wave fuzzy dark matter wormholes

Mohammad Alshammari[1,a], **M. Rizwan**[2,b], **Othman Abdullah Almatroud**[1,c], **M. Z. Bhatti**[2,3,d], **Saleh Alshammari**[1,e], **Z. Yousaf**[2,f]

[1] Department of Mathematics, College of Science, University of Ha'il, 2440 Ha'il, Saudi Arabia
[2] Institute of Mathematics, University of the Punjab, Lahore 54590, Pakistan
[3] Research Center of Astrophysics and Cosmology, Khazar University, 41 Mehseti Street, 1096 Baku, Azerbaijan

Received: 20 December 2025 / Accepted: 31 January 2026

Abstract In this manuscript, we study and construct minimally deformed fuzzy dark matter wormhole (WH) configurations fenced by solitonic quantum wave (SQW) dark matter (DM) halos using the minimal geometric deformation technique within the realm of Einstein's general theory of relativity. We construct the deformed spacetime by using SQW profile and test the obtained solutions against an extensive analysis concerning the shape function, embedding surfaces, mass distribution, compactness, and the fate of the effective equation of state. Moreover, we examine the conservation laws, the complexity function arising from anisotropic matter sources, and spacetime regularity to evaluate the physical validity of the model. Further, we pay particular attention to the satisfaction or violation of the classical energy conditions and their connection with the specific amount of exotic matter incorporated within the model as characterized by the parameter of exoticity and the corresponding volume integral quantifier. It is shown that within the framework of the MGD approach, traversable WH geometries are feasible, which smoothly capture the characteristics of SQW DM while showing an appropriate level of finely tuned exoticity within the vicinity of the throat.

1 Introduction

General relativity (GR) is considered the bedrock of contemporary gravitational physics and was proposed by Einstein in 1915. It describes gravity with fully geometrical terms in place of forces; from this point of view, its most important feature is the equivalence between the concepts of inertial and gravitational mass. This brings about the gravitational dynamics through the Einstein field equations (EFE), with curvature being related to the energy–momentum (EM) of the matter content. Contrary to Newton's gravity, GR allows for nonlinear interactions, dynamic geometries, exact solutions describing black holes (BHs), wormholes (WHs), gravitational waves, and compact stars, among cosmological models [1]. Such a predictive power has been empowered by the incredibly high experimental and observational accuracy starting from the perihelion shift of Mercury up to the very recent gravitational wave detection and high-resolution BH imaging. On the other hand, GR has also provided an appropriate arena for dealing with anisotropic fluids, exotic sources of matter, scalar fields, no-go dark matter (DM) distributions, and quantum-inspired corrections, so that it represents a sufficiently flexible theory for astrophysical and cosmological modeling [2,3].

The altered theories of gravity introduce novel geometrical, scalar, vector, or higher-dimensional aspects, beyond the gravitational part introduced originally by Einstein's GR, with purposes to explain phenomena that are not accessible to GR. These modifications, including, among others, $f(R)$ gravity [4], scalar–tensor theories [5], Gauss–Bonnet and Lovelock gravities [6–8], Braneworld theories [9], and Massive gravity [10], introduce variations to EFE, making possible a higher dynamics to be explored both for space-

[a] e-mail: dar.alshammari@uoh.edu.sa
[b] e-mail: mrizwan.math@gmail.com
[c] e-mail: o.almatroud@uoh.edu.sa
[d] e-mail: mzaeem.math@pu.edu.pk
[e] e-mail: saleh.alshammari@uoh.edu.sa
[f] e-mail: zeeshan.math@pu.edu.pk (corresponding author)

Published online: 17 February 2026

times and matter sources. Such approaches have already been utilized to explain phenomena, including cosmic acceleration, dark energy, curve of galaxies, and also to explore whether it is possible to have exotic objects, all independently of any source associated with unknown matter types. In regards to WHs, modifications to gravity can potentially provide solutions to keep these objects traversable, reducing and focusing violations to EC, making such objects more physically acceptable. Approaches like the MGD technique can be viewed as effective tools inspired by these theories, providing a systematic way to deform known GR solutions and investigate the resulting physical and geometric properties under alternative gravitational dynamics.

Wormholes are hypothetical solutions of EFE which describe tunnel-like geometries that connect two disjoint regions of spacetime; they may join two distant parts of the same universe or even different universes. Originally proposed by Einstein and Rosen in 1935 as the "Einstein–Rosen bridge" [2], these geometries have been first suggested to give a model for elementary particles and to study non-trivial spacetime topologies. The term "wormhole" has been later coined by Wheeler [11], with an emphasis on their role as spacetime shortcuts, and subsequent work by Ellis [12] and Morris and Thorne [13] rigorously formulated the concept of traversable WHs suitable for human or particle travel. Some of their key features include: throat structure connecting two asymptotically flat or curved regions, redshift function determining the absence of event horizons, shape function satisfying flare-out condition at the throat. Often, they need exotic matter to hold the throat and prevent collapse, where classical EC like null EC may be violated. Geometry for WHs is generally static and spherically symmetric, though rotation and dynamical solutions have been pursued extensively. However, their importance extends not only to theoretical explorations of causality, time travel, and topological features of spacetime but also to their potential astrophysical applications, such as gravitational lensing, DM interactions, and as probes of alternative or modified gravity theories.

Recent developments in WH physics have improved our understanding of the properties of exotic spacetime geometries, particularly in the presence of DM halos, altered theories of gravity, and quantum corrections. Among the early breakthroughs regarding the observational and constructive features of WHs, Dai and Stojkovic [14,15] explored the possibility of the observation of WH signatures and mechanisms due to their formation within relativistic settings. Subsequent investigations added spin, torsion, and quantum corrections to the study of violations of the null EC, given by Di Grezia et al. [16], showing how geometric properties at the microscopic level affect macroscopic traversability. Similarly, the impact of extended gravity has garnered deep interest; by using the Poynting–Robertson effect, De Falco and co-authors [17] were able to place constraints on WH solutions, establishing possible astrophysical tests in non-Einsteinian environments. More modern work has focused on the construction of WHs sustained by various DM density profiles: Einasto, fuzzy, and Zhao-type halos [18–20] yield new classes of traversable geometries which, under specific configurations, reduce or localize the amount of exotic matter. This set of works-from dark-halo-supported WHs in $4D$ Einstein–Gauss–Bonnet gravity [21] through structures developed in $f(R)$, $f(Q)$, and higher-order curvature theories [22–24] and models constructed in Einstein–Cartan and fuzzy dark matter frameworks [25,26] collectively showed that DM distributions can considerably affect WH stability, complexity, and geometric deformation. These discussions highlights that under certain circumstances matter fields, dark sources, and modified gravity interact in ways that create physically plausible WH structures compatible with theoretical restrictions and observational limitations.

In literature many scientists have focused on the WH stability, analysis of EC, gravitational lensing effects, and geometric properties in standard as well as altered theories of gravity [27–29]. It is important to note that many analyses have been performed to address the astrophysical aspects of WHs, existing in a galactic environment by Övgün et al. [30–32] in regards to their lensing properties and evolution inside DM halos. Important progress has been made by Yousaf et al. [33–35] by constructing WH models inspired by DM models characterized by the use of DM distributions with low geometric complexities and cylindrical sources complemented by global monopole charges. These analyses have demonstrated that DM distributions can be used to reduce the demands for exotic matter as well as maintain WH traversability. More recent analyses have focused on the role of geometric modifications and altered gravity theories. Analyses by Malik et al. [22] and Asad et al. [36] have shown that $f(R)$ and $\mathcal{F}(Q)$ models allow for WH solutions with relaxed or partially satisfied ECs. Furthermore, analyses have been performed on WH stability, geometric complexity minimization, and relativistic effects [37,38].

The MGD approach and the more general framework of gravitational decoupling (GD) have nowadays become powerful techniques for the generation of new and physically meaningful solutions to EFE. Introduced and formalized by Ovalle [39,40], the MGD method provides a systematic way for extending an arbitrary isotropic or perfect-fluid solution into an anisotropic domain while preserving its geometric structure. Important developments and applications of the technique have been presented in [41–43] by Casadio et al. who described its role in the analysis of black strings, solar system tests, and extended gravitational sectors. Subsequent developments came with Gabbanelli et al. [44] and with Las Heras and León [45], who showed that MGD describes in a controlled and transparent way the generation of anisotropic stellar configurations with an improved physical behavior.

Other contributions to the formalism, such as models of compact stars, BHs, and geometries with string clouds, have been explored in [46,47] by Ovalle et al., Panotopoulos and Rincón [48], and by Casadio et al. [49], which proves the versatility and predictive strength of the technique.

Recent analyses have extended the MGD method to DM contexts and WH physics. Almatroud et al. [50] adopted the MGD in anisotropic WHs enveloped by DM halos, proving the approach useful for describing both exoticity localization and EC behavior near the throat. Similarly, Yousaf et al. [51] used the Einasto density profile in order to model fuzzy DM-inspired BHs by gravitational decoupling, proving that MGD is capable of embedding realistic distributions of astrophysical matter. These results agree with previous theoretical extensions, such as the anisotropic models by Ovalle et al. [52], and further strengthen the role of GD as a powerful approach to deforming and coupling any number of gravitational sectors. In summary, the MGD is mathematically elegant and physically meaningful, since it generates realistic and stable anisotropic configurations, compact objects, BHs, and traversable WHs, which would be inaccessible by traditional analytical methods.

This article is organized in the following way: Sect. 2 provides the gravitational decoupling approach and the determination of the modified shape function through the introduction of SQW DM density as the temporal component of Θ-sector, along with the analysis of embedding surface, EC, and the volume integral quantifier. Section 3 addresses the characteristics and diagnostic parameters of the WH, including effective equation of state (EoS), conservation equation, compactness, gravitational mass, anisotropy factor, exoticity parameter, spacetime regularity and the complexity factor. Finally, Sects. 4 and 5 provide the summary and the concluding remarks, respectively.

2 MGD-decoupling and anisotropic wormholes

In this section, we describe the theoretical framework of the MGD approach to produce WH configurations within the context of SQW DM halo. We start by considering the EFE and the anisotropic EM tensor. Then we break down the matter distribution into two gravitational sources: a standard sector and an extra decoupled source, which we name $\Theta_{\psi\eta}$. The modification of the spacetime geometry generated by this extra source alters the EFE, giving birth to novel anisotropic configurations suited for WH geometries.

2.1 EFE and anisotropic matter content

The EFE in relativistic units ($8\pi G/c^4 = 1$) are given by

$$\mathbb{G}_{\psi\eta} = \mathbb{R}_{\psi\eta} - \frac{1}{2}\mathbb{R}g_{\psi\eta} = \mathbb{T}_{\psi\eta}, \tag{1}$$

where $\mathbb{G}_{\psi\eta}$ is the Einstein tensor, $\mathbb{R}_{\psi\eta}$ is the Ricci tensor, $\mathbb{R}$ is the scalar curvature, and $\mathbb{T}_{\psi\eta}$ denotes the EM tensor.

For an anisotropic fluid configuration, the EM tensor takes the form

$$\mathrm{T}_{\psi\eta} = (\hat{\Psi} + \hat{P}_t)u_\psi u_\eta + \hat{P}_t g_{\psi\eta} + (\hat{P}_r - \hat{P}_t)\chi_\psi \chi_\eta, \tag{2}$$

where $\hat{\Psi}$ is the energy density, $\hat{P}_r$ is the radial pressure, $\hat{P}_t$ is the tangential pressure, u_ψ is the timelike four-velocity ($u_\psi u^\psi = -1$), and χ_ψ is the radial unit four-vector.

2.2 Gravitational decoupling and EMT splitting

The GD method allows the EM distribution to be separated into two contributions [39,52]

$$\mathbb{T}_{\psi\eta} = \mathrm{T}_{\psi\eta} + \beta\Theta_{\psi\eta}, \tag{3}$$

where $\mathrm{T}_{\psi\eta}$ represents the standard matter sector and $\Theta_{\mu\nu}$ corresponds to an additional gravitational source coupled through a dimensionless parameter β. When $\beta = 0$, the system reduces to the original anisotropic configuration.

Substituting Eq. (3) into Eq. (1) yields

$$\mathbb{G}_{\psi\eta} = \mathrm{T}_{\psi\eta} + \beta\Theta_{\psi\eta}. \tag{4}$$

2.3 Spherically symmetric spacetime and MGD transformation

We consider the general static spherically symmetric line element

$$ds^2 = -e^{2\mathbb{C}(r)}dt^2 + \left(1 - \frac{\mathbb{E}(r)}{r}\right)^{-1} dr^2 + r^2\left(d\theta^2 + \sin^2\theta\, d\phi^2\right), \tag{5}$$

where $\mathbb{C} = \mathbb{C}(r)$ and $\mathbb{E} = \mathbb{E}(r)$ are the redshift and shape functions respectively. By solving equations (3) and (5) following fields equation will be obtained

$$\Psi = \hat{\Psi} + \beta\Theta_0^0 = \frac{\mathbb{E}'}{r^2}, \tag{6}$$

$$\mathbb{P}_r = \hat{P}_r - \beta\Theta_1^1 = -\frac{\mathbb{E}}{r^3}, \tag{7}$$

$$\mathbb{P}_t = \hat{P}_t - \beta\Theta_2^2 = \frac{\mathbb{E} - r\mathbb{E}'}{2r^3}, \tag{8}$$

where Ψ, $\mathbb{P}_r$ and $\mathbb{P}_t$ are the total or effective matter variables. The Eqs. (6)–(8) are independent of the redshift function $\mathbb{C}$, as we have taken $\mathbb{C} = constant$ to avoid event horizon and ensure traversable WH configurations. In the MGD approach, only the radial metric component is deformed:

$$\mathbb{E}(r) \implies \hat{\mathbb{E}}(r) + \beta\mathbb{D}(r), \tag{9}$$

where $\hat{\mathbb{E}}(r)$ corresponds to the undeformed seed solution (generated by $\mathrm{T}_{\psi\eta}$), while $\mathbb{D}(r)$ represents the geometric deformation produced by the additional source $\Theta_{\psi\eta}$.

Substituting Eq. (9) into the EFE leads to a decoupling of the EFE into:

Seed sector $\mathrm{T}_{\psi\eta}$:

$$\hat{\Psi} = \frac{\hat{\mathbb{E}}'}{r^2}, \tag{10}$$

$$\hat{P}_r = -\frac{\hat{\mathbb{E}}}{r^3}, \tag{11}$$

$$\hat{P}_t = \frac{\hat{\mathbb{E}} - r\hat{\mathbb{E}}'}{2r^3}. \tag{12}$$

For seed EM tensor $\mathrm{T}_{\psi\eta}$ conservation equation takes the following form

$$\nabla_\psi \mathrm{T}^\psi_\eta = 0 \implies -\hat{P}_r' - \frac{2}{r}(\hat{P}_r - \hat{P}_t) = 0. \tag{13}$$

Decoupled Θ-sector:

$$\Theta^0_0 = \frac{\mathbb{D}'}{r^2}, \tag{14}$$

$$\Theta^1_1 = -\frac{\mathbb{D}}{r^3}, \tag{15}$$

$$\Theta^2_2 = \frac{-\mathbb{D} + r\mathbb{D}'}{2r^3}, \tag{16}$$

with conservation equation

$$\nabla_\psi \Theta^\psi_\eta = 0 \implies -\Theta^{1'}_1 - \frac{2}{r}(\Theta^1_1 - \Theta^2_2) = 0. \tag{17}$$

These relations show how the additional source modifies the geometry, giving rise to anisotropy even if the seed matter distribution is isotropic. Due to their independent functioning, both components, $\Theta_{\psi\eta}$ and $\mathrm{T}_{\psi\eta}$, are gravitationally coupled. It should also be noted that the Θ-sector is conserved as a result of the conservation of $\mathbb{G}_{\psi\eta}$ and $\mathrm{T}_{\psi\eta}$. Bianchi's identities imply

$$\nabla_\psi \mathbb{G}^\psi_\eta = 0 \implies \nabla_\psi \mathrm{T}^\psi_\eta = 0, \tag{18}$$

which implies

$$\nabla_\psi \mathrm{T}^\psi_\eta + \beta\nabla_\psi \Theta^\psi_\eta = 0. \tag{19}$$

There are two possible interpretations of the zero on the right side of equation (19): (i) $\nabla_\psi \mathrm{T}^\psi_\eta = \nabla_\psi \Theta^\psi_\eta = 0$, or (ii) $\nabla_\psi \mathrm{T}^\psi_\eta = -\beta\nabla_\psi \Theta^\psi_\eta$. The former shows that there is just gravitational interaction between the sources since each source is covariantly conserved. The second choice denotes an energy exchange between both sources (see [108] for further information on this topic). We are put in case (i) under the current scenario. Furthermore, it is easy to verify that Eq. (17) is a linear combination of the field Eqs. (14)–(16). The hydrostatic equations that describe the configuration's balance are equations (13) and (17).

2.4 Relevance to wormhole construction

Since we are interested in examining the effects of GD via MGD on a WH spacetime, the well-known Morris–Thorne (MT) solution is considered as the so-called seed solution in this instance [13,53].

$$ds^2 = diag\left\{-1, \left(1 - \frac{r_0^2}{r^2}\right)^{-1}, r^2, r^2\, sin^2\theta\right\}, \tag{20}$$

The equation above shows that $\hat{\mathbb{E}} = \frac{r_0^2}{r}$ and $\hat{\mathbb{C}} = 0$. Within the context of the MGD solution, the spacetime (20) is chosen as the seed solution produced by the source $T_{\psi\eta}$. The shape function $\hat{\mathbb{E}} = \frac{r_0^2}{r}$ obeys the throat constraints $\hat{\mathbb{E}}(r_0) = r_0$ and $\hat{\mathbb{E}}'(r_0) = -1 < 1$, thus ensuring the satisfaction of flare-out condition at the throat of WH. The EFE yields the following expressions for the energy density and radial pressure corresponding to seed source $T_{\psi\eta}$.

$$\hat{\Psi} = \frac{\hat{\mathbb{E}}'}{r^2} = -\frac{r_0^2}{r^4}, \quad \hat{P}_r = -\frac{\hat{\mathbb{E}}}{r^3} = -\frac{r_0^2}{r^4}. \tag{21}$$

Therefore, the null EC for the seed sector $T_{\psi\eta}$ is breached,

$$\left(\hat{\Psi} + \hat{P}_r\right)\Big|_{r=r_0} = -\frac{2}{r_0^2} < 0, \tag{22}$$

and demonstrates that the source $T_{\psi\eta}$ supporting the MT WH geometry necessarily represents an exotic matter sector. In the MGD construction, this exotic seed configuration gives the background WH structure, whereas additional gravitational contributions come from the decoupled Θ-sector through the deformation parameter β, which in this case permits a redistribution of the total exoticity without removing the fundamental requirement imposed by the flaring-out condition. The MT spacetime (20) takes on the following form when the generic minimum deformation provided by equation (9) is taken into consideration.

$$ds^2 = diag\left\{-1, \left(1 - \frac{r_0^2}{r^2} - \frac{\beta\mathbb{D}}{r}\right)^{-1}, r^2, r^2\, sin^2\theta\right\}, \tag{23}$$

Naturally, the solution (20) is recovered when $\beta = 0$ in (20). Finding the decoupler function $\mathbb{D}(r)$ connected to the Θ-sector is now the primary goal. In theory, there are two methods to do this: either by solving the Θ-sector, taking into account a relationship between the $\Theta_{\psi\eta}$ components, or by fixing one of them. The first method involves imposing an appropriate deformation function $\mathbb{D}$. We will use the second choice in this situation.

As is generally known, a number of ideas have been taken into consideration to effectively shut or resolve the so-called Θ-sector [39,54]. In this instance, we select a particular kind for the temporal component of the Θ-sector. Specifically, we will suppose the so-called SQW energy density of a static, spherically symmetric, gravitational source [55]. Being the ground-state solution of the Schröder-Poisson system, the solitonic DM density profile arises naturally in wave-like or ultralight scalar-field theories of DM [56,57]. It can generally be written as

$$\Theta_0^0 = \Psi_0 \left[1 + \alpha \left(\frac{r}{r_c}\right)^2\right]^{-n}, \tag{24}$$

where Ψ_0 is the central density, r_c is the core radius and the parameters (α, n) specify a unique form for the solitonic core. For the standard fuzzy DM soliton, these are generally given by $\alpha \simeq 0.091$ and $n = 8$ [58]. A distinctive feature of wave DM, this profile has a smooth finite-density central core, a sharp suppression at large radii, and it follows the scaling equation $\Psi_0 \propto r_c^{-4}$. Due to its providing of a universal structural connection between the solitonic core and its host halo, such a profile is very important, and it also gives a resolution of small-scale discrepancies of the ΛCDM paradigm, for example, the core-cusp problem [59,60]. The comparison of equations (14) and (24) yields the following differential equation

$$\frac{\mathbb{D}'}{r^2} = \Psi_0 \left(\frac{\alpha r^2}{r_c^2} + 1\right)^{-n}, \tag{25}$$

with solution

$$\mathbb{D} = c + \frac{1}{3}\Psi_0 r^3 \, {}_2F_1\left(\frac{3}{2}, n; \frac{5}{2}; -\frac{r^2\beta}{r_s^2}\right) \tag{26}$$

where the decoupler function $\mathbb{D}$ meets the condition $\mathbb{D}(r_0) = 0$ because the non-deformed function already satisfies the condition $\hat{\mathbb{E}}(r_0) = r_0$. So

$$\mathbb{D}(r_0) = 0 \implies c = -\frac{1}{3}\Psi_0 r_0^3 \, {}_2F_1\left(\frac{3}{2}, n; \frac{5}{2}; -\frac{\alpha r_0^2}{r_s^2}\right), \tag{27}$$

this implies

$$\mathbb{D} = \frac{1}{3}\Psi_0 r^3 \, {}_2F_1\left(\frac{3}{2}, n; \frac{5}{2}; -\frac{r^2\xi}{s^2}\right) - \frac{1}{3}\Psi_0 r_0^3 \, {}_2F_1\left(\frac{3}{2}, n; \frac{5}{2}; -\frac{\alpha r_0^2}{r_s^2}\right). \tag{28}$$

The MT spacetime will become

$$ds^2 = diag\left\{-1, \left(1 - \frac{r_0^2}{r^2} - \frac{\beta\Psi_0}{3r}\left(r^3 \, {}_2F_1\left(\frac{3}{2}, n; \frac{5}{2}; -\frac{r^2\xi}{s^2}\right) - r_0^3 \, {}_2F_1\left(\frac{3}{2}, n; \frac{5}{2}; -\frac{\alpha r_0^2}{r_s^2}\right)\right)\right)^{-1}, r^2, r^2 \, sin^2\theta\right\}. \tag{29}$$

The modified shape function is given by,

$$\mathbb{E} = \frac{1}{3}\beta\Psi_0 r^3 \, {}_2F_1\left(\frac{3}{2}, n; \frac{5}{2}; -\frac{r^2\xi}{s^2}\right) - \frac{1}{3}\beta\Psi_0 r_0^3 \, {}_2F_1\left(\frac{3}{2}, n; \frac{5}{2}; -\frac{\alpha r_0^2}{r_s^2}\right) + \frac{r_0^2}{r}. \tag{30}$$

By substituting the value of the modified shape function $\mathbb{E}$ into the field Eqs. (6)–(8), we get the following expressions for effective matter variables.

$$\Psi = \beta\Psi_0 \left(\frac{\alpha r^2}{r_s^2} + 1\right)^{-n} - \frac{r_0^2}{r^4}, \tag{31}$$

$$\mathbb{P}_r = \frac{1}{3r^r}\left\{\beta\mu_0 r^4 \, {}_2F_1\left(\frac{3}{2}, n; \frac{5}{2}; -\frac{r^2\alpha}{r_s^2}\right) - \beta\Psi_0 r_0^3 r \, {}_2F_1\left(\frac{3}{2}, n; \frac{5}{2}; -\frac{\alpha r_0^2}{r_s^2}\right) + 3r_0^2\right\}, \tag{32}$$

$$\mathbb{P}_t = \frac{1}{6}\left\{-\frac{\beta\Psi_0 r_0^3}{r^3} \, {}_2F_1\left(\frac{3}{2}, n; \frac{5}{2}; -\frac{\alpha r_0^2}{r_s^2}\right) + \beta\Psi_0 \times \left({}_2F_1\left(\frac{3}{2}, n; \frac{5}{2}; -\frac{r^2\alpha}{r_s^2}\right) - 3\left(\frac{\alpha r^2}{r_s^2} + 1\right)^{-n}\right) + \frac{6r_0^2}{r^4}\right\}. \tag{33}$$

The graphical depiction of the modified shape function is given in Fig. 1. In the graphical analysis of modified shape function $\mathbb{E}$, governed by the decoupling parameter β, one sees how the underlying solitonic DM profile determines the WH geometry. For large β this makes the core of the configuration less concentrated and $\mathbb{E}$ flattened, shifting the throat radius outward, which reflects the weakening gravitational weight of the DM soliton as it decouples. Its derivative $\mathbb{E}'$ correspondingly decreases, but always $\mathbb{E}'(r_0) < 1$, an important condition for the flare-out of the WH throat. Similarly, direct calculation shows that the flare-out term remains positive near r_0, signaling a continued violation of

the null EC necessary for traversability. The metric functions $1-\mathbb{E}/r$ and $\mathbb{E}/r$ further illustrate that the spacetime is smooth and horizonless: the former is positive outside the throat, while the latter goes to zero for large r [61]. Increasing β stretches the WH throat through the quantum pressure of the soliton, increasing the region of exotic matter that keeps the passage open without introducing singularities or horizons.

We further examine the so-called embedding diagram to confirm the asymptotically flat nature of the solutions. Therefore, pertinent details regarding the shape of the WH structure can be obtained from the generic line element (20). The embedding diagram represents a simple geometric method of displaying the spatial structure of a WH spacetime [53]. It is obtained by embedding a two-dimensional equatorial slice of the WH metric, taken at constant time, into a higher dimensional Euclidean space. In the case of a static and spherically symmetric WH, the embedding diagram gives a clear picture of how the throat joins two asymptotically flat regions of spacetime. It is important because it makes the curvature of space intuitive, and provides an immediate way of seeing whether the geometry meets the flaring-out condition necessary for traversable WH to exist. The physical importance of the embedding surface lies in how it reflects the fact that the obtained shape function controls the geometry near the throat and that the presence of the matter or effective stresses is necessary to keep the WH open. A smooth and well-behaved embedding surface indicates the absence of horizons or singular behavior. Stronger curvature close to the throat is correlated with a stronger gravitational field [13,61]. Therefore, the embedding diagram could be a straightforward and helpful way to evaluate the geometrical consistency and physical plausibility of WH models. When focusing on an equatorial plane, $\theta=\pi/2$, the solid angle element Ω^2 becomes

$$\Omega^2=d\phi^2. \tag{34}$$

Additionally, when $t=constant$ is fixed, the line element (20) becomes

$$ds^2=\left\{1-\frac{\mathbb{E}}{r}\right\}^{-1}dr^2+r^2d\phi^2. \tag{35}$$

It is useful to think about cylindrical coordinates in order to view the equatorial plane as a two-dimensional surface encrusted in a three-dimensional Euclidean space.

$$ds^2=dz^2+dr^2+r^2d\phi^2, \tag{36}$$

which can also be written as

$$ds^2=\left\{1+\left(\frac{dz}{dr}\right)^2\right\}dr^2+r^2d\phi^2. \tag{37}$$

The comparison of Eqs. (35) and (37) yields

$$\frac{dz}{dr}=\pm\left\{\frac{r}{\mathbb{E}}-1\right\}^{-1/2}, \tag{38}$$

where the embedded surface is defined by the function $z=z(r)$. Since $\mathbb{E}$ is finite in the limit $r\longrightarrow\infty$, the expression (38) translates to [13,53,61]

$$dz/dr\mid_{r\to+\infty}=0. \tag{39}$$

This indicates that two asymptotically flat regions are covered by the WH spacetime. However, expression (38) may result in a different situation in this instance. Thus, considering (13) one has

$$dz/dr=\pm\left\{\frac{r}{\hat{\mathbb{E}}+\beta\mathbb{E}}-1\right\}^{\frac{-1}{2}}. \tag{40}$$

To visualize the WH geometry, we have constructed the embedding diagrams using numerical methods implemented in Python (as depicted in Fig. 2). Although symbolic computation software like Mathematica is often employed to solve such tasks, the solitonic DM density profile prevents finding a closed-form solution for the integral defining the embedding function. For this task, Python allows us to evaluate this integral with high precision by taking advantage of its robust numerical libraries. The graphs in this study depict smooth, high-resolution representations of WH surfaces. The obtained graphs convincingly indicate how the upper and lower universes are connected through the throat; they exhibit the characteristic flaring-out behavior expected from traversable WHs. This graph indeed confirms the regularity of the geometry near the throat and provides intuitive insight into the features of the change in the WH shape exerted by the solitonic density-features which would be challenging to capture analytically.

A new parameter in the MGD approach, named decoupling parameter β, represents the degree of gravitational coupling of the MT seed $T_{\psi\eta}$ source itself with the new or additional Θ-sector describing the SQW DM halo. The parameter β does not describe a new independent matter coupling constant but has a phenomenological character as a measure of the relative efficiency of the solitonic core contribution compared to the seed source of exotic matter. The SQW DM cores are described by a finite central density, a regular pressure distribution, and a smooth decay along the radial coordinate, and their gravitational effects are dominant in the inner halo

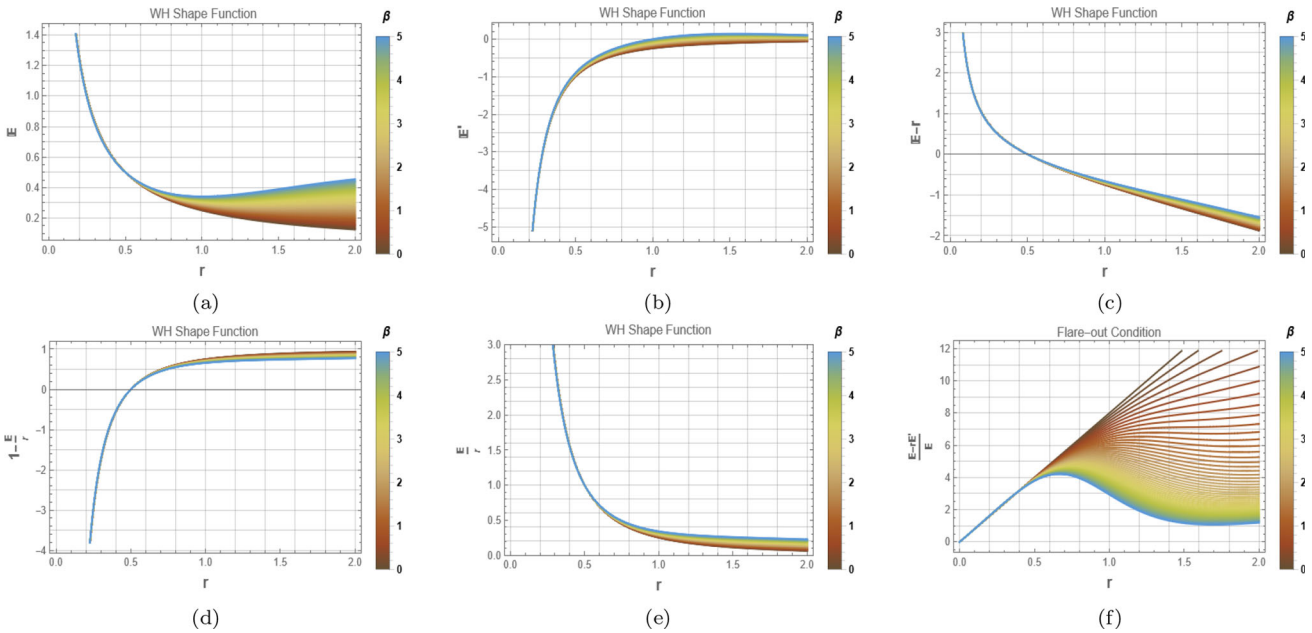

Fig. 1 Graphical behavior of the modified shape function $\mathbb{E}$ and other associated curves for the parametric values $r_s = 1$, n=8, $r_0 = 0.5$, $\Psi_0 = 0.1$, $\alpha = 0.091$ and various decoupling parameter β

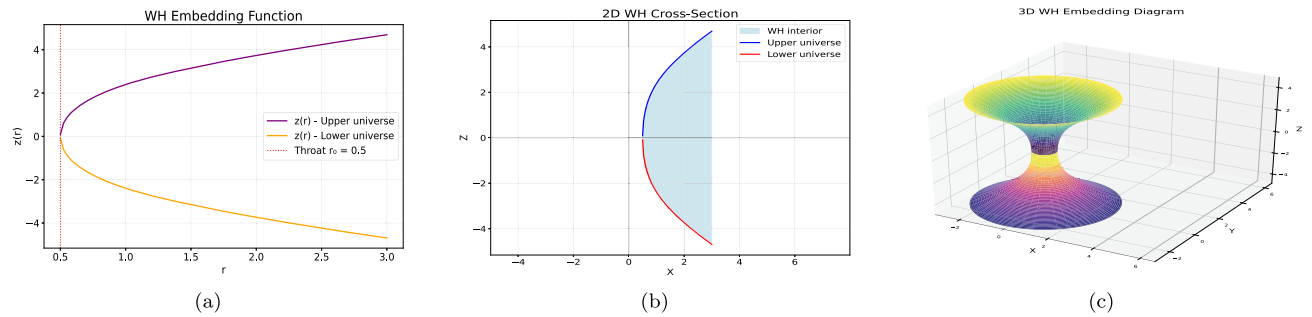

Fig. 2 WHs embedding diagram for the parametric values $r_s = 1$, $n = 8$, $r_0 = 0.5$, $\Psi_0 = 0.1$, $\alpha = 0.091$ and various decoupling parameter β

parts [58–60]. As a consequence, moderate values for β are allowed, and large coupling constants would imply an unrealistic deformation of the WH geometry, being inconsistent with the smooth and self-gravitating nature of solitonic cores. The range $0 \leq \beta \leq 5$ is therefore chosen to fulfill the following physical and geometric conditions:

1. the preservation of the WH throat and the flaring-out conditions,
2. the regularity of the effective energy density and pressures, and
3. compatibility with the characteristic scale and strength of SQW DM cores.

In this range, the Θ-sector offers a controlled and physically well-motivated contribution to the curvature of spacetime, in order to allow a partial redistribution of the exoticity needed in the seed source.

2.5 Energy Conditions and Volume Integral Quantifier

The EC play a central role in the investigation of physical viability of the matter distribution by GR. They are given as a set of inequalities imposed on the EM tensor and aimed to represent reasonable classical matter behavior. In WH physics, they took particular importance. Namely, at least the null EC violation is necessary to maintain the traversable WH throat. Concretely, the flaring-out condition at the throat gives the inequality $\Psi + \mathbb{P}_r < 0$ close to the throat, signaling the presence of some kind of exotic matter or effective stresses not describable by ordinary classical fluids. Such violations are inevitable in standard GR; however, their degree and localization are of great importance from the physical point of view. A large number of viable WH models were able to confine EC violations to a small region close to the throat or to reinterpret them by means of an effective matter sources coming from modified gravity theories. Thus, EC analysis provides

an essential diagnostic tool in understanding the nature, the distribution, and the physical acceptability of the matter at hand necessary to support the geometrical WH settings.

Figure 3 and Table 1 above depicts how the different EC respond for a decoupled SQW WH solution with $r_s = 1$, $n = 8$, $r_0 = 0.5$, $\Psi_0 = 0.1$, and $\alpha = 0.091$ for varying decoupling parameter β. Panel (3a) shows how $\Psi + \mathbb{P}_r$ is always negative in a small region around the throat, violating the null EC but satisfying the requirement for maintaining a WH. As it goes further away from the throat in the positive r-direction, $\Psi + \mathbb{P}_r$ approaches 0 from below, which shows a localized and diminishing effect in violating this EC. Panel (3b) shows that $\Psi + \mathbb{P}_t$ in a small region around the throat is positive for most decoupling parameters β and decreases to 0 in the positive r-direction, indicating a partial relief in the exotic matter effect supplied by the radial null EC. Of course, such an alleviation does not contradict the need for this exotic matter support in maintaining a WH geometry. Panel (3c) shows how $(\Psi + \mathbb{P}_r) + 2\mathbb{P}_t$ is always non-negative in a region far from the throat, thus satisfying this particular EC in most regions of space. Therefore, these observations highlight a decoupling parameter effect where part of this exotic matter requirement is localized in a small region in and around the throat and how it returns a spacetime configuration towards a more standard behavior at a larger r scale.

In order to investigate if the SQW sector of the DM, introduced by the parameter β of the MGD, succeeds in minimizing the amount of exotic matter required in maintaining the WH, it is crucial to distinguish between seed and effective sources. Despite the seed being supported by the MT geometry, which has the manifestation of intrinsically exotic matter in the form of $T_{\psi\eta}$, the effective matter present in the spacetime is given by the equation

$$\Psi = \hat{\Psi} + \beta\,\Theta_0^0, \quad P_r = \hat{P}_r - \beta\,\Theta_1^1. \tag{41}$$

One way of quantifying the notion of exoticity is the null EC combination,

$$\Xi(r) \equiv \hat{\Psi} + \hat{P}_r, \tag{42}$$

which is strictly negative at the throat for the seed sector, $\Xi(r_0) < 0$, as required by the flaring-out condition. When the decoupled Θ-sector is activated, the associated effective amount becomes

$$\Xi^{\text{eff}}(r) = \Psi + P_r = \left(\hat{\Psi} + \hat{P}_r\right) + \beta\left(\Theta_0^0 - \Theta_1^1\right). \tag{43}$$

For the SQW DM model under examination, the region for $\Theta_0^0 - \Theta_1^1$ is positive (or less negative) near the throat, which means that for higher β, $\Xi^{\text{eff}}(r)$ becomes less negative. Thus, the null EC continues to be violated to sustain the WH, but the amount of the violation decreases compared to the seed solution. This activity typifies that the SQW DM sector does not eliminate the requirement for exotic matter, but rather represents an equitable redistribution of the gravitational support for the WH. The value of β determines the measure of the overall curvature contributed by the Θ-sector, which in turn reduces the exoticity requirement incurred by the seed source $T_{\psi\eta}$. The activity represents the SQW DM halo, which implements the role of the stabilizing factor for the gravitational support, in an attempt to equate for the exotic matter introduced by the flaring-out condition. The decrease in exotic matter is further supported by the fact that the volume integral quantifier magnitude decreases as the value of β increases, clarifying that the total amount of exotic matter reduces in the background of the SQW DM sector.

The volume integral quantifier ($\mathbb{V}_{iq}$) is a global estimate of the total amount of exotic matter that is needed to maintain a certain WH solution. It is given by the integral of the amount of the EC violation over the volume of the WH, with emphasis on the vicinity of the WH throat where these EC violations are expected to be extreme. One of the important aspects of the $\mathbb{V}_{iq}$ is that it can be used to estimate not only the existence of exotic or effective stresses but also their distribution, thereby serving as a complementary analysis of the EC. In the context of SQW DM-WHs, the calculation of the $\mathbb{V}_{iq}$ is very important for identifying the extent to which EC violation is localized and can be reduced for physically viable solutions [62]. A smaller volume of exotic matter is desired, which would improve the viability of the solution with the aim of developing traversable and stable WH solutions in generalized theories of gravity like GR. It is defined as

$$\mathbb{V}_{iq} \equiv \int (\Psi + \mathbb{P}_r) dV = 2\int_{r_0}^{\infty} 4\pi(\Psi + \mathbb{P}_r) x^2 dx. \tag{44}$$

Figure 3d shows how the $\mathbb{V}_{iq}$ varies with the radial coordinate for different values of the decoupling parameter β. The $\mathbb{V}_{iq}$ gives a global idea of the total amount of EC violating matter necessary for maintaining the WH configuration. Looking at Fig. 3d, it can be observed that the volume integral quantifier approaches negative values for regions beyond the throat and continues to decay smoothly with an increase in radius, hence manifesting the presence of exotic matter in and around the throat region. Moreover, this decay shows a slow rate, with all these functions approaching stability at larger values of the radial coordinate, thus making it clear that the amount of exotic matter will not increase without bound. As expected, the effects of the decoupling parameter β can be seen in Fig. 3d with increasing values of β showing a mild increase in the level of exotic matter, yet maintaining a qualitative form in a manner similar to a standard graph. This manifestation shows that decoupling is capable of maintaining a controlled level of EC violations, hence effectively restricting the amount of

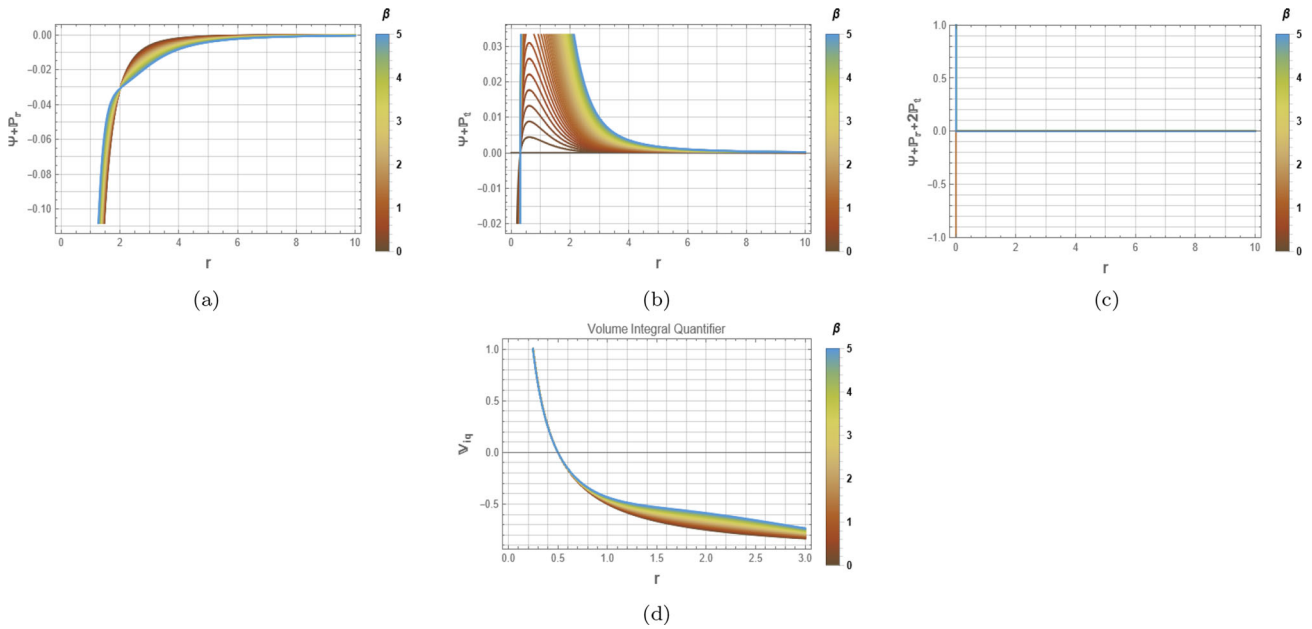

Fig. 3 Energy conditions and volume integral quantifier behavior for the parametric values $r_s = 1$, $n = 8$, $r_0 = 0.5$, $\Psi_0 = 0.1$, $\alpha = 0.091$ and various decoupling parameter β

Table 1 Violation region and behavior of EC for the decoupled SQW DM-WHs

Energy condition	Radial domain	Physical behavior
$\Psi + \mathbb{P}_r$ (radial null EC)	$r \lesssim r_0$	Violated near the throat, indicating exotic matter
	$r \gg r_0$	Gradually approaches zero (effective restoration)
$\Psi + \mathbb{P}_t$ (Tangential null EC)	Near throat	Mostly satisfied for admissible β values
	Large r	Smoothly tends to zero
$\Psi + \mathbb{P}_r + 2\mathbb{P}_t$ (strong EC)	Entire spacetime	Satisfied, ensuring global regularity for higher β

exotic matter within a certain region in and around the throat. Therefore, the SQW DM-modified WH solution is capable of maintaining a minimal amount of exotic matter, which greatly favors a physically feasible model.

3 Characteristic and diagnostic parameters of the wormholes

In this section, we discuss and test some important characteristic and diagnostic parameters associated with the WHs and describe the physical and structural viability of the obtained SQW DM-WH solutions.

3.1 Equation of state parameter

In the present analysis, the shape function of the WH geometry is determined directly from the SQW DM density profile, without appealing to any specific EoS. The EoS remains nevertheless an important diagnostic tool in understanding the physical nature of the matter threading the WH. After determining the metric functions and the various stress–energy components, effective radial and tangential EoS parameters can be constructed in terms of the form $\mathbb{W}_r = \mathbb{P}_r/\Psi$ and $\mathbb{W}_t = \mathbb{P}_t/\Psi$. The behaviour of these parameters describes the anisotropic character of the supporting matter and offers important diagnostics for deviations from standard fluids. In particular, the variations of $\mathbb{W}_r$ and $\mathbb{W}_t$ around the throat indicate the presence of exotic or effective stresses that sustain the WH structure, while their asymptotic behaviour at large distances determines whether the spacetime settles to a physically reasonable regime. Although the EoS is not used here to generate the shape function, it is essential for assessing the physical viability and interpretative consistency of the SQW DM-supported WH model.

The radial and tangential EoS has very different, but physically meaningful, dependencies across the interior of the WH for the values of the decoupling parameter β (as shown in Fig. 4). In the vicinity of the throat, the values of both EoS parameters remain finite, verifying the regularity of the SQW-

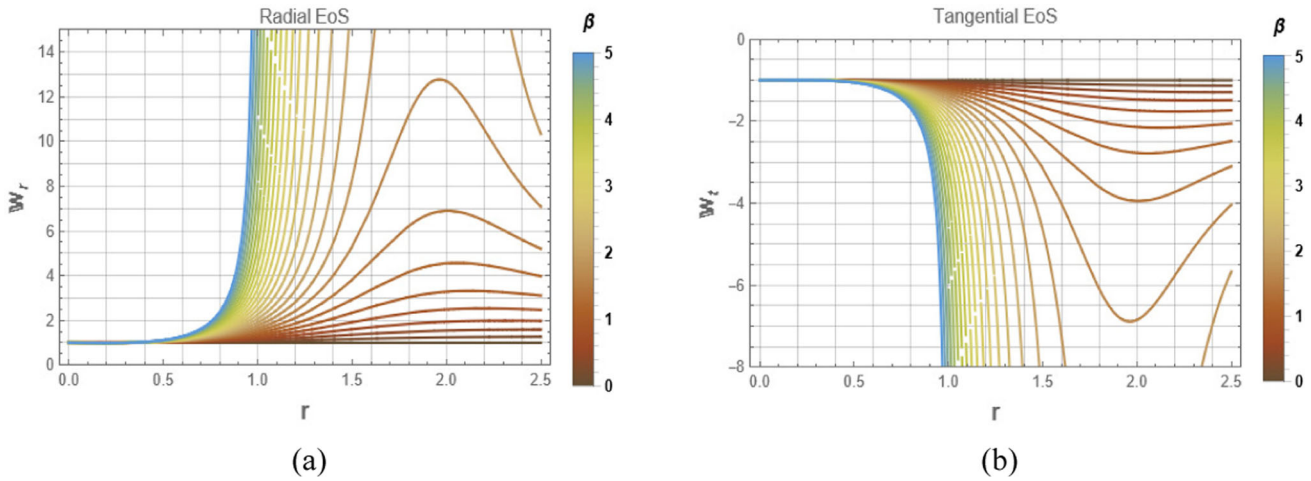

Fig. 4 Behavior of EoS parameters verses radial axis r for the parametric values $r_s = 1$, n=8, $r_0 = 0.5$, $\Psi_0 = 0.1$, $\alpha = 0.091$ and a range of decoupling parameter β

inspired DM distribution. The radial EoS parameter $\mathbb{W}_r$ (in Fig. 4(a)) is very β-dependent, remains nearly constant close to the throat and then increases rapidly along the radial axis r. This indicates the existence of the anisotropies away from the WH throat. The tangential EoS $\mathbb{W}_t$ shows the negative profile (as shown in Fig. 4(b)) which indicates the existence of an exotic core of the WH, and then rising rapidly with the radial coordinate toward higher negative values, especially for higher values of β, due to the dominant role of the anisotropic part produced with the help of MGD. The tangential EoS parameter $\mathbb{W}_t$ possess negative or weakly dependent values in the vicinity of the throat and more stabilized and less exotic values away from it. The significant difference between $\mathbb{W}_r$ and $\mathbb{W}_t$ shows the natural anisotropy caused by the decoupling field effect and proves the SQW DM-inspired source of the regular, controllable, and anisotropic pressure distribution supporting the WH configuration.

3.2 Conservation equation

The effective EM tensor conservation, universally expressed as $\nabla_\psi \mathbb{T}^\psi_\eta = 0$, results in the Tolman–Oppenheimer–Volkkoff (TOV) equation, describing self-gravitating systems at equilibrium. Within the framework of static and spherically symmetric WH solutions that consist of anisotropic matter, the TOV equation describes the balance of forces between three competitors: the gravitational force, hydrostatic force of pressure, and another force related to anisotropic pressures. As distinct from compact stellar systems, in which the gravitational force is always directed inwards, for WH solutions, the role of the gravitational force, contributing to their stability, can be directed outward in the vicinity of the throat, emphasizing the repulsive properties of exotic or effective matter that materialize the geometry of the solutions. A precisely balanced TOV equation is a sign of adequate stability of the WH solution with respect to gravitational collapses or developing any singular points [63,64].

$$\mathbb{P}'_r + \frac{\mathbb{C}'}{2}(\Psi + \mathbb{P}_r) + \frac{2(\mathbb{P}_r - \mathbb{P}_t)}{r} = 0. \tag{45}$$

where, $f_g = -\frac{\mathbb{C}'}{2}(\Psi + \mathbb{P}_r)$, $f_a = -\frac{2(\mathbb{P}_t - \mathbb{P}_r)}{r}$ and $f_h = -\frac{d\mathbb{P}_r}{dr}$ are the gravitational, anisotropic and hydrostatic forces respectively. Because of the constant redshift function, the gravitational influence is zero (i.e., $f_g = 0$). So, the equilibrium condition is given as $f_a + f_h = 0$.

Figure 5 shows the radial profiles of the conservative forces involved in the equilibrium of the decoupled WH system for various values of the decoupling parameter β. The positive radial component of the anisotropic force f_a throughout the interior of the WH confirms its outward orientation, which provides a balancing effect to the inward pull caused by the pressure gradient and hence plays a very important role in the stability of the anisotropic system. In the region around the throat, the magnitudes of the anisotropic force are very high and depend heavily on β; however, as the radial distance increases, the magnitude of this force drops drastically to almost negligible values in the radial region, showing a decrease in the overall effects of anisotropy at longer distances. The hydrostatic force component f_h, on the other hand, is always negative in the entire radial region, confirming its inward orientation. Its magnitudes are also largest near the throat region because of the dominant pressure gradients there; hence, they decrease smoothly in the radial direction and eventually tend to a constant value. The opposing characteristics of the graphic representations of f_a and f_h from each panel of Fig. 5 confirm that the outward-directed balance provided by the former exactly matches the hydrostatic force component of the system and hence con-

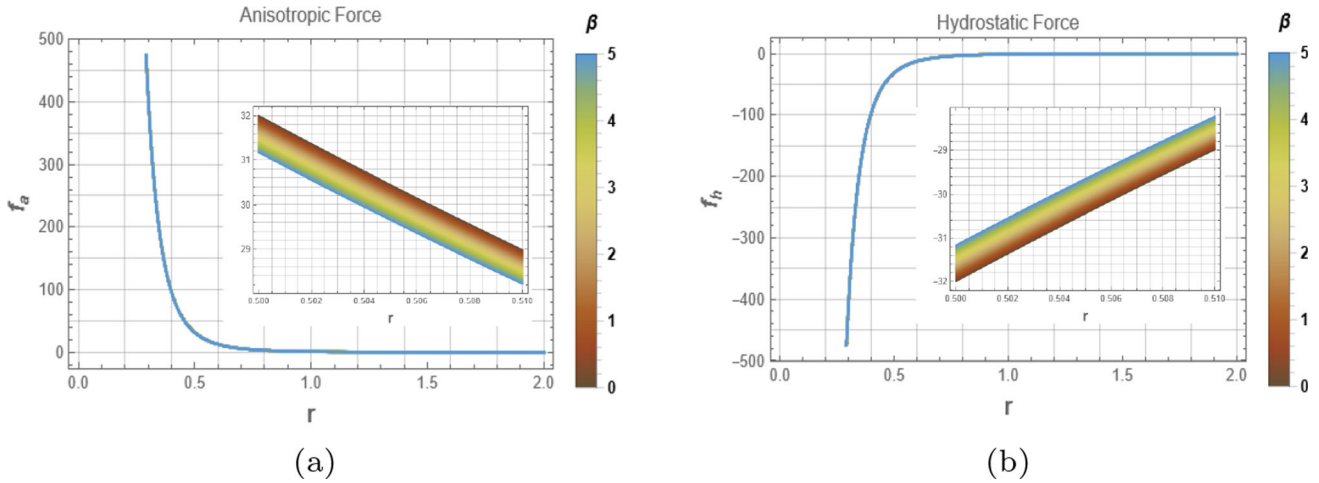

Fig. 5 Graphical depiction of conservative forces verses radial axis r for the parametric values $r_s = 1$, n=8, $r_0 = 0.5$, $\Psi_0 = 0.1$, $\alpha = 0.091$ and a range of decoupling parameter β

firms a very well-balanced system, ensuring a stable WH in this gravitational decoupling scenario.

3.3 Active gravitational mass and compactness of the WH

The concepts of compactness and active gravitational mass are useful metrics for defining the geometric strength and gravitational impact of WH spacetime. The active gravitational mass represents the effective mass enclosed within a given radial coordinate and is computed by integrating the energy density over the spatial volume. In the case of a WH, this quantity sums up the incoherent contribution due to matter and effective stresses that hold the throat and shape the geometry around it. Although the presence of exotic or anisotropic matter modifies the interpretation of mass compared with ordinary compact objects, the active gravitational mass remains a good indicator of how the WH deforms spacetime. Closely connected with the latter, the compactness parameter is defined as the ratio of the active gravitational mass to the radial coordinate [13]. Compactness is a dimensionless measure of the strength of the gravitational field and, at the same time, allows a direct comparison with other relativistic configurations. For a physically acceptable WH, the compactness is normally bounded and divergence-free, implying the absence of horizons and keeping the WH traversable. Altogether, active gravitational mass and compactness offer valuable insight into the global structure, gravitational behaviour, and physical acceptability of WH solutions sustained by SQW DM distributions. The active gravitational mass is defined as [21]

$$\mathbb{M} = 4\pi \int_{r_0}^{r} \omega^2 \Psi'(\omega) d\omega. \tag{46}$$

Figure 6 illustrates the active gravitational mass and its associated compactness ratio for the WH solution for varying decoupling parameter β. From Fig. 6a, it is clear that the enclosed mass $\mathbb{M}$ starts from a positive value near the throat region and smoothly depends on the radial parameter r. This smooth dependence of enclosed mass on the radial parameter ensures that there is no singularity in the mass distribution of the source, thus ensuring the physical acceptability of the solution. Moreover, it has been noticed that higher values of β produce a slight variation in the enclosed mass distribution, ensuring that the decoupled source makes a non-trivial contribution to the gravitational field of the source.

In Fig. 6b, the corresponding compactness factor $\mathbb{C}_p = \mathbb{M}/r$ is plotted, which depicts a monotonically decreasing behaviour with the increase in the radial distance r. The compactness measures the maximum value around the throat and monotonically decays to negligible values at large distances, thereby ensuring the avoidance of horizon formation around the spacetime. The effect of the decoupling parameter β indicates an increase in the compactness around the throat with raising β due to the reinforced gravitational interactions of the matter distribution arising from the decoupling of the anisotropic component. The joint study of the mass function and the compactness factor clearly indicates the gravitationally stable, horizon-free, and correct traversal of the constructed WH compatible with the expected decoupled SQW DM scenario of the traversable WH spacetime.

3.4 Anisotropy and exoticity parameters

The anisotropy and exoticity parameters play an important role in understanding the nature of the matter content needed to sustain a WH geometry. The anisotropy parameter, defined as the difference between the tangential and radial pres-

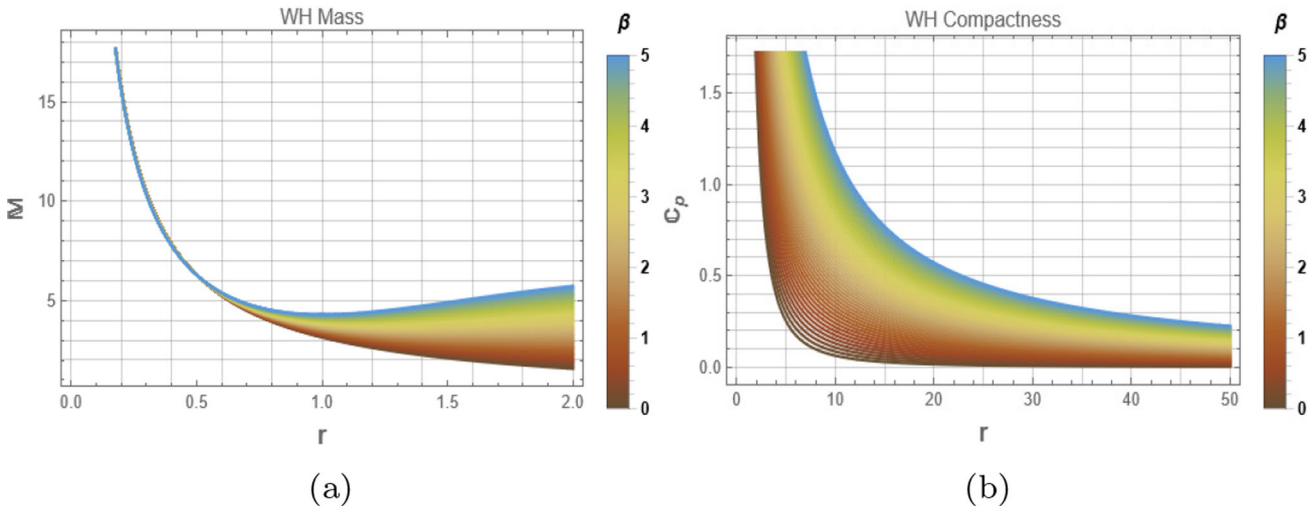

Fig. 6 Mass within the WH territory and compactness for $r_s = 1$, n=8, $r_0 = 0.5$, $\Psi_0 = 0.1$, $\alpha = 0.091$ and a range of decoupling parameter β

sures, characterizes the degree to which the stress distribution depends on direction and is linearly related to stability and equilibrium of the WH throat. In general, it is impossible to avoid anisotropy in WH spacetimes; rather, anisotropy furnishes the additional repulsive stress needed to counterbalance gravitational collapse [65]. The exoticity parameter, on the other hand, quantifies, in some sense, how much the matter content deviates from ordinary classical behavior. It has become customary to use this parameter to identify regions where the EC are violated, and it often occurs near the throat. For positive values of the exoticity parameter, the matter content is exotic or effective, thereby furnishing the pressure that supports the flaring-out condition, while negative values correspond to non-exotic regimes. Due to the importance of both parameters in characterizing the spacetime that supports the WH, the analysis of anisotropy and exoticity parameters helps in localizing and characterizing the region responsible for maintaining the WH structure, giving further insights into the physical viability of the models sustained by SQW DM distributions.

$$\Delta(r) = \mathbb{P}_t - \mathbb{P}_r. \tag{47}$$

Exoticity parameter is defined as

$$\mathbb{X}_x = -\frac{\mathbb{P}_r + \Psi}{|\Psi|}. \tag{48}$$

Figure 7 exhibits the radial behavior of the anisotropic factor and the exoticity parameter for different values of the decoupling parameter β. The plot in panel (7a) shows that the anisotropic factor Δ achieves significantly large positive values near the throat and decays very fast with increasing radial coordinate. This reflects the fact that near the throat, the contribution of tangential pressure becomes dominant to counterbalance the gravitational attraction in order to maintain the stability of the WH geometry. The inset plot zooms this fact into the smooth and controlled variation of anisotropy in the near-throat region as due to the constructive participation of the decoupled sector without any induction of instabilities. The β dependence further shows that the larger the value of the decoupling parameter is chosen close to the throat, the stronger the anisotropic effects which accomplish the flaring-out condition to achieve traversability.

Panel (7b) shows the exoticity parameter $\mathbb{X}_x$, a quantitative measure of the presence of exotic matter. It is readily seen that $\mathbb{X}_x$ takes positive values within a narrow area in the vicinity of the throat, reflecting that the null EC is necessarily violated in this region. The exoticity parameter decays with increasing radial distance and converges to smaller values, which means that the exotic matter content is indeed confined to a finite region around the throat. What is implied by the dependence on β is that the decoupling method enables precise dissemination of the exotic matter and hence reduces it to its minimum spatial extension, with the preservation of the WH integrity. These results further confirm that pressure anisotropy and exoticity, generated by the decoupled SQW DM sector, are actually essential and well-controlled ingredients for obtaining physically viable WH solutions.

3.5 Kretschmann scalar and singularity analysis

The Kretschmann scalar is a significant curvature invariant that helps in detecting the possibility of having spacetime singularities in relativistic geometry [66]. It is given by the contraction of the Riemann tensor, representing the total strength of the curvature in an independent manner. Within the framework of a WH spacetime geometry, the analysis of the Kretschmann scalar helps in ensuring that the geometry is

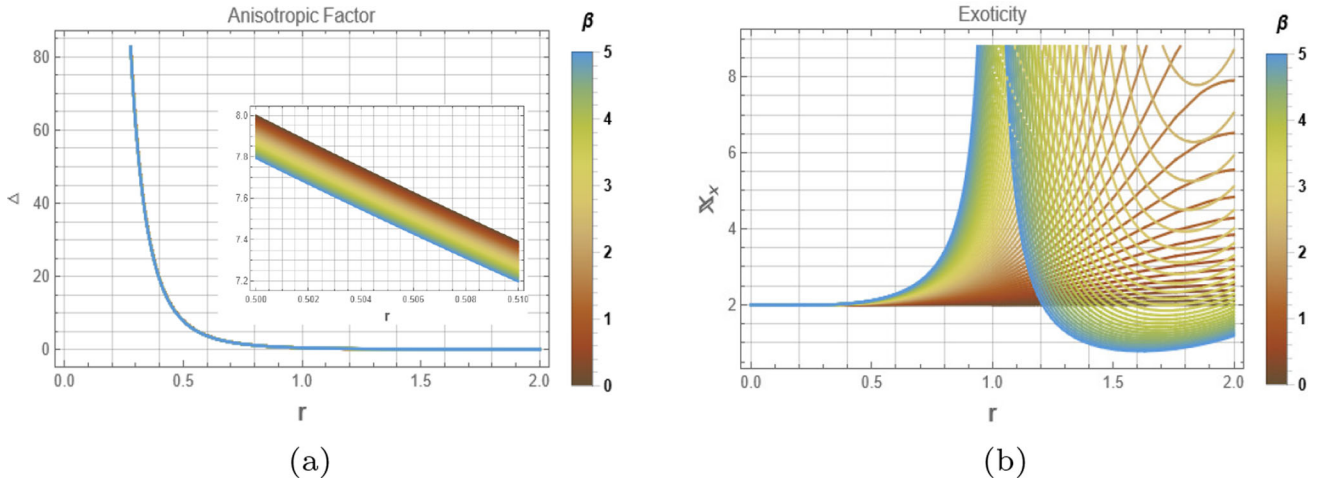

(a) (b)

Fig. 7 Anisotropic factor and Exoticity parameter corresponding to the parametric values $r_s = 1$, $n = 8$, $r_0 = 0.5$, $\Psi_0 = 0.1$, $\alpha = 0.091$ and a range of decoupling parameter β

devoid of any type of physical singularities, especially around the throat region [67,68]. A finite value of the Kretschmann scalar helps in ensuring that the WH solution is rimmed with no curvature singularities and that any type of singularity in the metric components is actually an artifact of the chosen coordinate system. This is of great importance in the context of anisotropic or exotic matter-based WH solutions that are expected to harbor strong curvature around the throat region. Therefore, the analysis of the Kretschmann scalar helps in ensuring that the geometry is consistent with the interpretation of a traversable WH solution [69–72]. It is defined as

$$\mathbb{K}_s = \mathbb{R}_{\phi\eta\mu\nu}\mathbb{R}^{\phi\eta\mu\nu}. \tag{49}$$

The complexity factor is supposed to give a quantitative measure of the internal structural complexity of a WH spacetime by combining inhomogeneity in energy density and anisotropy in pressure [73]. First proposed considering the orthogonal splitting of the Riemann tensor, this is represented by the structure scalar $\mathbb{Y}_{tf}$, which essentially encodes deviations from a simple homogeneous, isotropic setting. In WH models, the complexity factor helps in gauging how matter anisotropic stresses may combine to hold out the throat while maintaining equilibrium [74–76]. A vanishing or low value of the complexity factor will describe an balanced configuration in which the anisotropy and density gradients have balanced each other's effects and hence can minimize the need for exotic matter. In contrast, the higher the value of the complexity factor is, the stronger will the deviations from homogeneity be, signaling even more intricate internal structures that may impress on stability and traversability. Analysis of the complexity factor gives an important insight into geometric and physical properties of the WH sustained by the SQW DM distributions. It is defined as [77,78]

$$\mathbb{Y}_{tf} = 4\pi(\mathbb{P}_t - \mathbb{P}_r) + \frac{1}{r^3}\int_0^r y^3\Psi'(y)\,dy. \tag{50}$$

Figure 8 illustrates the radial dependence of the scalar of Kretschmann curvature and the complexity factor for various levels of the decoupling parameter β. In panel (8a), it can be seen that the scalar of Kretschmann curvature, $\mathbb{K}_s$, has finite values across spacetime and smoothly decreases with increasing radial distances. Even though it attains higher levels of magnitude near the WH throat, it neither becomes infinite nor leads to any curvature singularity across spacetime, thus clearing its regularity and confirming the absence of curvature singularities in this solution. Moreover, it is worthwhile to note that this behavior holds for various levels of decoupling parameter β. This clarifies that decoupled SQW DM sectors under different levels of the decoupling parameter β ensure regular spacetime with no possibility of singularities.

In panel (8b), the radial evolution of the complexity factor is depicted, which incorporates both the energy density inhomogeneity and pressure anisotropy. It is noted that the complexity factor reaches its maximum value at the vicinity of the throat and monotonically decreases with the increase in radial distance, finally attaining values barely sustainable from a distance away from the throat. This result clearly suggests that the inner structure of the WH is most complex at distances close to the vicinity of the throat, where both anisotropic pressure and geometric asymmetric features dominate. Additionally, from the inset graph, a smooth and well-managed variability in the complexity factor is noticed at closer distances from the throat. It is also revealed from the graph that higher values of the decoupling parameters β result in decreasing complexities, which clearly ensures the suitability and effectiveness of the decoupling process in the management of the inner structure of the WH.

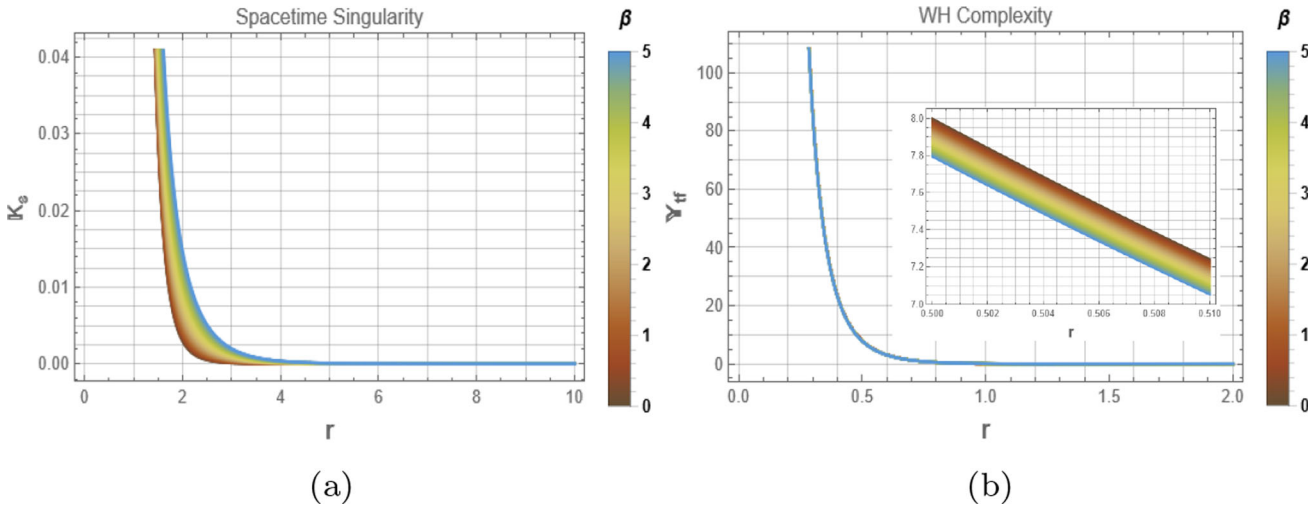

Fig. 8 Graphical analysis of spactime singularity and complexity factor for $r_s = 1$, n=8, $r_0 = 0.5$, $\Psi_0 = 0.1$, $\alpha = 0.091$ and a range of decoupling parameter β

4 Summary

The case of static and spherically symmetric WHs is studied in the context of GR and SQW DM. The analysis uses the MGD approach, which expresses the effective EM tensor as a sum of a standard source and a Θ-part, characterized by the SQW DM configuration. Without employing an EoS for the dark sector, the WH shape function $\mathbb{E}$ is directly calculated using the SQW density, providing a physically motivated and self-consistent solution for the geometry of the gravitating spacetime. The physical and geometric acceptability of the solution is checked using a number of indicators. The EC demonstrate that the null EC is violated only near the throat of the WH, necessary for its traversability, but otherwise remaining well-behaved with growing distances. The estimator of the integral volume discriminates the solution as a physically acceptable one, indicating a finite, arbitrarily small amount of exotic matter. Equilibrium for the solution is guaranteed by the TOV equation, with an essential role of anisotropic stresses for stabilizing the solution. The analysis of the EoS parameters, embedding surfaces, anisotropies, and estimators of exoticness, as well as active gravitational mass and compactness of the solution, supports further the acceptability of the obtained solution for the geometry of gravitating spacetime with SQW dark sector. The quality of the spacetime is verified to be regular as the finiteness of the Kretschmann scalar is established. Moreover, the complexity factor shows that the complexity of the wormhole core is very complex and diminishes as one moves far away from the wormhole core. This outcome shows that decoupled SQW DM is a useful framework to construct the physically acceptable WHs.

5 Conclusion

In this work we have presented the complete investigation of static and spherically symmetric decoupled WH solutions which arise from SQW DM distribution in the framework of GR. Gravitational decoupling method was implemented, splitting the total EM tensor in an effective seed source plus additional Θ-sector, but providing at the same time the SQW DM profile, being a physical motivated source, which shapes the WH geometry. The result obtained satisfies every geometrical fundamental requirement for a traversable WH, including throat condition and the flaring-out criterion (as depicted in Fig. 1). A closer inspection of the EC showed that the null EC is necessarily violated within some narrow region surrounding the WH throat, which is an unsurprising and unavoidable characteristic shared by all traversable WHs spacetime. We observed that this violation is bounded and regulated by the decoupling parameter β, while the effective matter content tends to satisfy the EC away from the throat (as shown in Fig. 3). This localized violation emphasizes the role of the decoupled SQW DM sector as the minimal amount of exotic ingredient required for the maintenance of the WH structure. We further studied the volume integral quantifier ($\mathbb{V}_{iq}$) and found that the integral converges to a finite, negative, and relatively small value, which means that the total exotic content can, in principle, be arbitrarily small by an appropriate choice of model parameters (see Fig. 3(f)).

Although the shape function was constructed directly from the SQW density profile rather than an assumed EoS, the effective radial and tangential EoS were discussed in order to gain insight into the behavior of the supporting matter fields. It follows that a smooth radial evolution of the EoS parameters is registered, without unphysical diver-

gences (see Fig. 4). Also, the generalized TOV conservation equation confirms that the WH configuration remains in static equilibrium under the combined action of hydrostatic, and anisotropic forces, with anisotropy playing a crucial stabilizing role (see Fig. 5 for graphical visualization). The geometric properties of the WH were further elucidated through the embedding surface analysis. The embedding diagrams show the characteristic flaring geometry near the throat in an intuitively clear manner, displaying several features typical for WHs (as shown in Fig. 2). Given the complexity of the analytical expressions resulting from the SQW DM source, the embedding surfaces were constructed numerically using Python; this proved to be very robust and effective. This approach gave us the ability to represent those important geometrical features that would otherwise be unreachable by purely analytical methods. The graphical behavior of active gravitational mass and compactness of the obtained solutions (as shown in Fig. 6), supports further the acceptability of the obtained solution for the geometry of gravitating spacetime with SQW dark sector.

The study of anisotropy factor and the exoticity parameter, in tiniest detail, showed that the pressure anisotropy is strongest near the throat and decreases smoothly with the radial distance. The sign of the exoticity parameter keeps positive in the vicinity of the throat, as a proof that the exotic matter exists there where its existence is strictly required, and goes negative or negligible at bigger radii (as can be seen in Fig. 7). This behavior means, as far as interpretation of results goes, that the decoupled SQW DM sector is responsible for sustaining the WH without introducing widespread exotic behavior. The regularity and internal structure of the spacetime were finally probed by using the Kretschmann scalar and the complexity factor (as shown in Fig. 8). The Kretschmann scalar is bounded everywhere in the spacetime and, hence, proves that the curvature singularities are absent and the WH geometry is regular. On the other hand, the complexity factor attains its maximum near the throat and decreases monotonically outward; this shows that the inner part of the WH, where the effects of anisotropy and DM are predominant, corresponds to the most structurally complicated region of the WH. Altogether, these results establish decoupled SQW DM as a consistent, well–behaved, and physically motivated arena for creating viable WH solutions.

Data Availability Statement This manuscript has no associated data. [Authors' comment: Data sharing not applicable to this article as no datasets were generated or analysed during the current study.].

Code Availability Statement This manuscript has no associated code/software. [Authors' comment: Code/Software sharing not applicable to this article as no code/software was generated or analysed during the current study.].

Declarations

Conflict of interest The authors have no Conflict of interest with respect to the publication of the present paper.

Funded by SCOAP[3].

References

1. R.M. Wald, *General Relativity* (University of Chicago Press, Chicago, 2010)
2. A. Einstein, N. Rosen, The particle problem in the general theory of relativity. Phys. Rev. **48**, 73 (1935)
3. J.R. Oppenheimer, H. Snyder, On continued gravitational contraction. Phys. Rev. **56**, 455 (1939)
4. T.P. Sotiriou, V. Faraoni, $f(R)$ theories of gravity. Rev. Mod. Phys. **82**, 451 (2010)
5. D. Ross, Scalar–tensor theory of gravitation. Phys. Rev. D **5**, 284 (1972)
6. D. Glavan, C. Lin, Einstein–Gauss–Bonnet gravity in four-dimensional spacetime. Phys. Rev. Lett. **124**, 081301 (2020)
7. T. Padmanabhan, D. Kothawala, Lanczos–Lovelock models of gravity. Phys. Rep. **531**, 115 (2013)
8. Z. Yousaf, Viscous fluid cosmology: a path to cosmic acceleration. Phys. Dark Univ. **48**, 101884 (2025)
9. R. Maartens, K. Koyama, Brane-world gravity. Living Rev. Relativ. **13**, 5 (2010)
10. K. Hinterbichler, Theoretical aspects of massive gravity. Rev. Mod. Phys. **84**, 671 (2012)
11. J.A. Wheeler, Geons. Phys. Rev. **97**, 511 (1955)
12. H.G. Ellis, Ether flow through a drainhole: a particle model in general relativity. J. Math. Phys. **14**, 104 (1973)
13. M.S. Morris, K.S. Thorne, Wormholes in spacetime and their use for interstellar travel: a tool for teaching general relativity. Am. J. Phys. **56**, 395 (1988)
14. D.-C. Dai, D. Stojkovic, Observing a wormhole. Phys. Rev. D **100**, 083513 (2019)
15. D.-C. Dai, D. Minic, D. Stojkovic, How to form a wormhole. Eur. Phys. J. C **80**, 1103 (2020)
16. E. Di Grezia, E. Battista, M. Manfredonia, G. Miele, Spin, torsion and violation of null energy condition in traversable wormholes. Eur. Phys. J. Plus **132**, 537 (2017)
17. V. De Falco, E. Battista, S. Capozziello, M. De Laurentis, Testing wormhole solutions in extended gravity through the Poynting-Robertson effect. Phys. Rev. D **103**, 044007 (2021)
18. Z. Yousaf, M. Rizwan, M. Alshammari, O.A. Almatroud, S. Alshammari, M.M. Al-sawalha, Wormholes construction through

the diverse dark matter density profiles. Eur. Phys. J. C **85**, 998 (2025)
19. Z. Yousaf, M. Z. Bhatti, M. Rizwan, J. Rayimbaev, I. Ibragimov, I. Davletov, From dark halos to exotic bridges: wormhole structures with Einasto density profiles. Nucl. Phys. B **1019**, 117128 (2025)
20. S. Khan, H.M.A. Mahmoud, Zhao profile-based black holes embedded in fuzzy halos under Hu–Sawicki $f(R)$ gravity. Phys. Dark Univ. **49**, 102053 (2025)
21. Z. Hassan, P.K. Sahoo, Possibility of the traversable wormholes in the galactic halos within 4d Einstein–Gauss–Bonnet gravity. Ann. Phys. **536**, 2400114 (2024)
22. A. Malik, T. Naz, A. Qadeer, M.F. Shamir, Z. Yousaf, Investigation of traversable wormhole solutions in modified $f(R)$ gravity with scalar potential. Eur. Phys. J. C **83**, 522 (2023)
23. M. Tayde, P.K. Sahoo, Wormhole formations in the galactic halos supported by dark matter models and global monopole charge within $f(Q)$ gravity. Eur. Phys. J. Plus **139**, 774 (2024)
24. M. Yousaf, H. Asad, A. Rehman, M. Shahzad, J. Rayimbaev, E. Davletov, Imprints of global monopole charge on the stability and energy conditions of traversable wormholes in $f(R)$ gravity. Phys. Dark Univ. **50**, 102123 (2025)
25. Z. Yousaf, M. Rizwan, M. Alshammari, O.A. Almatroud, S. Alshammari, M.M. Al-sawalha, Minimally complex fuzzy wormhole models in Einstein–Cartan theory of gravity. Phys. Dark Univ. **50**, 102082 (2025)
26. Z. Yousaf, K. Bamba, B. Almutairi, M. Z. Bhatti, M. Rizwan, Fuzzy dark matter less-complex wormhole structures in higher-order curvature gravity. Nucl. Phys. B **1018**, 116997 (2025)
27. V. De Falco, E. Battista, S. Capozziello, M. De Laurentis, General relativistic Poynting- Robertson effect to diagnose wormholes existence: static and spherically symmetric case. Phys. Rev. D **101**, 104037 (2020)
28. V. De Falco, E. Battista, S. Capozziello, M. De Laurentis, Reconstructing wormhole solutions in curvature based extended theories of gravity. Eur. Phys. J. C **81**, 157 (2021)
29. E. Battista, S. Capozziello, A. Errehymy, Generalized uncertainty principle corrections in Rastall–Rainbow casimir wormholes. Eur. Phys. J. C **84**, 1314 (2024)
30. A. Övgün, Evolving topologically deformed wormholes supported in the dark matter halo. Eur. Phys. J. Plus **136**, 1 (2021)
31. K. Jusufi, A. Övgün, Gravitational lensing by rotating wormholes. Phys. Rev. D **97**, 024042 (2018)
32. A. Övgün, M. Halilsoy, Existence of traversable wormholes in the spherical stellar systems. Astrophys. Space Sci. **361**, 214 (2016)
33. Z. Yousaf, B. Almutairi, M. Rizwan, T. Ganesan, M. Z. Bhatti, Modeling less complex fuzzy dark matter cylindrical wormholes. Int. J. Mod. Phys. D **34**, 2450072 (2025)
34. Z. Yousaf, A. Adeel, M. Rizwan, G. Mustafa, A. Ali, Construction of complexity-free fuzzy dark matter wormholes. Int. J. Geom. Methods Mod. Phys. **22**, 2550093 (2025)
35. M. Alshammari, M. Rizwan, O. Almatroud, S. Alshammari, Z. Yousaf, Stability assessment of fuzzy wormhole structures in $\mathcal{F}(Q)$ gravity theory having global monopole charge. Int. J. Geom. Methods Mod. Phys. (2025). https://doi.org/10.1142/S021988782650009X
36. H. Asad, M. Yousaf, U. Zafar, J. Rayimbaev, A. Dauletov, Traversable wormholes in $f(R)$ gravity: influence of global monopole charge and energy conditions. Fortschr. Phys. **73**, e70034 (2025)
37. M. Yousaf, B.S. Alkahtani, G. Mustafa, S.K. Maurya, Interpretation of conservative Morris–Thorne type topologically charged wormhole models and energy conditions with relativistic corrections. Chin. J. Phys. **97**, 1255 (2025)
38. O.A. Almatroud, M. Rizwan, M. Z. Bhatti, M. Alshammari, S. Alshammari, Z. Yousaf, Electromagnetic fields and fuzzy wormholes. Phys. Dark Univ. **50**, 102135 (2025)
39. J. Ovalle, Decoupling gravitational sources in general relativity: from perfect to anisotropic fluids. Phys. Rev. D **95**, 104019 (2017)
40. J. Ovalle, Decoupling gravitational sources in general relativity: the extended case. Phys. Lett. B **788**, 213 (2019)
41. R. Casadio, J. Ovalle, R. Da Rocha, Black strings from minimal geometric deformation in a variable tension brane-world. Class. Quantum Gravity **31**, 045016 (2014)
42. R. Casadio, J. Ovalle, R. Da Rocha, Classical tests of general relativity: brane-world sun from minimal geometric deformation. Europhys. Lett. **110**, 40003 (2015)
43. R. Casadio, J. Ovalle, R. Da Rocha, The minimal geometric deformation approach extended. Class. Quantum Gravity **32**, 215020 (2015)
44. L. Gabbanelli, Á. Rincón, C. Rubio, Gravitational decoupled anisotropies in compact stars. Eur. Phys. J. C **78**, 370 (2018)
45. C. Las Heras, P. León, Using MGD gravitational decoupling to extend the isotropic solutions of Einstein equations to the anisotropical domain. Fortschr. Phys. **66**, 1800036 (2018)
46. J. Ovalle, A. Sotomayor, A simple method to generate exact physically acceptable anisotropic solutions in general relativity. Eur. Phys. J. Plus **133**, 428 (2018)
47. J. Ovalle, R. Casadio, R.D. Rocha, A. Sotomayor, Z. Stuchlík, Black holes by gravitational decoupling. Eur. Phys. J. C **78**, 960 (2018)
48. G. Panotopoulos, Á. Rincón, Minimal geometric deformation in a cloud of strings. Eur. Phys. J. C **78**, 851 (2018)
49. R. Casadio, E. Contreras, J. Ovalle, A. Sotomayor, Z. Stuchlik, Isotropization and change of complexity by gravitational decoupling. Eur. Phys. J. C **79**, 826 (2019)
50. O.A. Almatroud, M. Rizwan, M. Alshammari, M. Z. Bhatti, S. Alshammari, Z. Yousaf, Decoupling of anisotropic wormholes via mgd in the presence of dark matter haloes. Eur. Phys. J. C **85**, 1285 (2025)
51. Z. Yousaf, S. Khan, B. Almutairi, T. Ganesan, M. Z. Bhatti, Gravitationally decoupled fuzzy black holes inspired by einasto density profile. Chin. J. Phys. **97**, 210 (2025)
52. J. Ovalle, R. Casadio, R. Da Rocha, A. Sotomayor, Anisotropic solutions by gravitational decoupling. Eur. Phys. J. C **78**, 122 (2018)
53. M.S. Morris, K.S. Thorne, U. Yurtsever, Wormholes, time machines, and the weak energy condition. Phys. Rev. Lett. **61**, 1446 (1988)
54. G. Abellán, V. Torres-Sánchez, E. Fuenmayor, E. Contreras, Regularity condition on the anisotropy induced by gravitational decoupling in the framework of MGD. Eur. Phys. J. C **80**, 1 (2020)
55. R.C. Pantig, A. Övgün, Black hole in quantum wave dark matter. Fortschr. Phys. **71**, 2200164 (2023)
56. H.-Y. Schive, T. Chiueh, T. Broadhurst, Cosmic structure as the quantum interference of a coherent dark wave. Nat. Phys. **10**, 496 (2014)
57. A. Herrera-Martín, M. Hendry, A.X. Gonzalez-Morales, L.A. Ureña-López, Strong gravitational lensing by wave dark matter halos. Astrophys. J. **872**, 11 (2019)
58. H.-Y. Schive, M.-H. Liao, T.-P. Woo, S.-K. Wong, T. Chiueh, T. Broadhurst, W.P. Hwang, Understanding the core-halo relation of quantum wave dark matter from 3d simulations. Phys. Rev. Lett. **113**, 261302 (2014)
59. J.F. Navarro, C.S. Frenk, S.D. White, A universal density profile from hierarchical clustering. Astrophys. J. **490**, 493 (1997)
60. G.G.L. Nashed, W.E. Hanafy, Stable soliton dark matter wormhole in non-minimally coupled $f(\mathcal{Q},\mathcal{T})$ gravity. J. Cosmol. Astropart. Phys. **09**, 040 (2025)
61. M. Visser, *Lorentzian Wormholes. From Einstein to Hawking* (Woodbury, New York, 1995)
62. K.K. Nandi, Y.-Z. Zhang, K.V. Kumar, Volume integral theorem for exotic matter. Phys. Rev. D **70**, 127503 (2004)

63. R.C. Tolman, Static solutions of Einstein's field equations for spheres of fluid. Phys. Rev. **55**, 364 (1939)
64. J.R. Oppenheimer, G.M. Volkoff, On massive neutron cores. Phys. Rev. **55**, 374 (1939)
65. L. Herrera, N.O. Santos, Local anisotropy in self-gravitating systems. Phys. Rep. **286**, 53 (1997)
66. A.D. Rendall, The nature of spacetime singularities, in *100 Years of Relativity: Space-time Structure: Einstein and Beyond* (World Scientific, Singapore, 2005), p. 76
67. S.W. Hawking, G.F. Ellis, *The Large Scale Structure of Space-Time* (Cambridge University Press, Cambridge, 2023)
68. J.M. Senovilla, Singularity theorems and their consequences. Gen. Relativ. Gravit. **30**, 701 (1998)
69. J. Earman, Tolerance for spacetime singularities. Found. Phys. **26**, 623 (1996)
70. C.B. Collins, G.F.R. Ellis, Singularities in Bianchi cosmologies. Phys. Rep. **56**, 65 (1979)
71. G.F. Ellis, B.G. Schmidt, Singular space-times. Gen. Relativ. Gravit. **8**, 915 (1977)
72. P.S. Joshi, *Gravitational Collapse and Spacetime Singularities* (Cambridge University Press, Cambridge, 2007)
73. L. Herrera, Entropy **23**, 802 (2021)
74. L. Herrera, A. Di Prisco, J. Carot, Complexity of the Bondi metric. Phys. Rev. D **99**, 124028 (2019)
75. L. Herrera, A. Di Prisco, J. Ospino, Complexity factors for axially symmetric static sources. Phys. Rev. D **99**, 044049 (2019)
76. H.M.A. Mahmoud, S. Khan, L. Abdalgadir, Anisotropic stellar fluids with zero complexity factor in torsion-inspired gravity. Phys. Dark Univ. **49**, 101974 (2025)
77. L. Herrera, A. Di Prisco, J. Ospino, Definition of complexity for dynamical spherically symmetric dissipative self-gravitating fluid distributions. Phys. Rev. D **98**, 104059 (2018)
78. L. Herrera, New definition of complexity for self-gravitating fluid distributions: the spherically symmetric, static case. Phys. Rev. D **97**, 044010 (2018)